RSC Advances

ROYAL SOCIETY OF CHEMISTRY

www.rsc.org/advances

Plasmonic Z-Scheme α/β-Bi_2O_3-Ag-AgCl Photocatalyst with Enhanced Visible-Light Photocatalytic Performance

Huijie Cheng,[a] Jungang Hou,[ab]* Hongmin Zhu,[ab] Xing-Min Guo[a]*

[a]School of Metallurgical and Ecological Engineering, University of Science and Technology Beijing, Beijing 100083, China

[b]Tohoku University, 6-6-02 Aramaki-Aza-Aoba, Aoba-ku, Sendai, 980-8579 Japan

E-mail: jhou@ustb.edu.cn (J. Hou); guoxm@metall.ustb.edu.cn (X. Guo)

Abstract:

Environmental treatment over bismuth based catalysts due to its appropriate band structure and abundance is a promising process. However, the practical application of single-phase bismuth based catalysts is hindered by serious charge transport limitations. The plasmonic Z-scheme α/β-Bi_2O_3–Ag–AgCl photocatalysts resolving the drawbacks of single-component photocatalyst have been successfully synthesized by anchoring Ag–AgCl nanocrystals on the surfaces of α/β-Bi_2O_3 nanowire heterojunction via the deposition–precipitation method in assistance with the photo-reduction process. The as-prepared samples were characterized by a series of techniques, such as X-ray diffraction (XRD), electron microscopy (EM), Brunauer-Emmett-Teller analysis (BET), and UV-vis diffuse reflectance absorption spectra (UV-vis). The effects of the amount and the photo-reduction time of Ag–AgCl nanocrystals upon the photocatalytic performance for the α/β-Bi_2O_3–Ag–AgCl composites were systematically investigated. Inspiringly, the plasmonic α/β-Bi_2O_3–Ag–10wt%AgCl–30 composites exhibit the superior photocatalytic performance than

α/β-Bi_2O_3 nanowires over the degradation of rhodamine B and acid orange 7 dyes due to the effective charge transfer between Ag–AgCl nanocrystals and α/β-Bi_2O_3 nanowires. On the basis of photocatalytic activity and band structure analysis, a plasmonic Z-scheme photocatalytic mechanism is proposed; namely, two-step visible-light absorption is caused by the localized surface plasmon resonance of metallic Ag nanocrystals and the band gap photoexcitation of α/β-Bi_2O_3. This work could provide new insights into the fabrication of plasmonic Z-scheme photocatalysts with high performance and facilitate their practical application in environmental remediation issues.

Keywords: Ag–AgCl nanocrystals; α/β-Bi_2O_3 nanowires; Photocatalyst; Degradation

1. Introduction

Environmental problems associated with harmful organic pollutants in water are the driving forces for sustained fundamental and applied research in the area of environmental remediation on the basis of highly efficient semiconductor photocatalysts.[1-5] To date, a large number of metal oxides as photocatalysts have been explored for the purpose of efficient degradation of harmful organic substances and hydrogen production through splitting water.[6-10] To date, TiO_2, as a semiconductor photocatalyst with large band gap (about 3.2 eV), has been intensively investigated under UV irradiation. However, titania can only absorb about less than 5% of sunlight.[1] Recently, TiO_2 has been modified by transition-metal cations, non-metal anions (such as N, S, C, F) or noble metal nanoparticles for the improvement of the catalytic performance in the visible range.[11-14] Furthermore, the bismuth based multimetal oxides with a $6s^2$ configuration, such as $CaBi_2O_4$,[15] $BiVO_4$,[16] Bi_2WO_6,[17] Bi_3NbO_7[2,4,18] and $Bi_{12}TiO_{20}$,[19-23] have shown to be active under visible illumination, which is ascribed to the fresh-constructed, well-dispersed

valence bands by the hybridization of Bi 6s and O 2p orbitals.[24]

As is known, Bi_2O_3, as a semiconductor catalyst, possesses high photocatalytic performance under visible-light irradiation due to the appropriate band gap.[25] Generally, Bi_2O_3 has four different polymorphs, denoted as monoclinic α, tetragonal β, body-centered cubic γ, and face-centered cubic δ, among which, the low-temperature α-phase and the high-temperature δ-phase are stable; while the other two phases are high-temperature metastable.[26] Though many researches on α-Bi_2O_3 have been reported, there was only a few on β-Bi_2O_3, in most of which β-Bi_2O_3 was obtained due to the difficulty of the synthesis of this metastable phase.[27-33] Recently, Muruganandham *et al*. have successfully used two types of bismuth oxalates as a precursor for various morphological Bi_2O_3 preparations.[34] Brezesinski *et al*. found that the mesoporous β-Bi_2O_3 showed the exceptional photocatalytic activity.[35] Huang *et al*. prepared bismuth oxide nanoparticles were synthesized directly via a liquid phase microwave reaction.[36] To the best of our knowledge, it is therefore highly desirable to develop a new modification and/or preparation method that can enhance the photocatalytic performance of the Bi_2O_3 nanostructures.

To improve the photocatalytic performance, a novel strategy has been applied via the constructing hierarchical nanostructures for photocatalytic applications by anchoring functional species on semiconductors.[37] The surface plasmon resonance of metal nanoparticles has been introduced to the photocatalysts due to the enhanced absorption in the visible light region.[38,39] For examples, Ag/AgX/BiOX (X = Cl, Br) three-component photocatalysts were synthesized by a low-temperature chemical bath method.[40] Dai *et al*. precipitated Ag/AgCl on P25 to synthesize Ag/AgCl/TiO_2 catalysts for the environmental remediation of Cr(VI) and organic dyes.[41] Currently, Ag/AgCl@WO_3,[42] Ag/AgBr/TiO_2,[43] Ag/AgX/GO (X = Cl, Br),[44] Ag/AgCl/ZnO,[45] Ag/AgCl/titanate honeycomb,[46] Ag/AgCl/BiOCl,[47] Ag/AgCl/TaON,[48] AgX/Ag_3PO_4 (X = Cl, Br, I),[49] have also been

investigated. Thus, there appears to be great untapped potential for exploring the improvement of photocatalytic activity of α/β-Bi_2O_3–Ag–AgCl composites using plasmonic Ag–AgCl nanocrystals.

In this work, the influences of the synthesis parameters on the resulting products, the synthesis mechanism, the critical roles of treatment conditions and catalyst compositions in determining catalytic performance, as well as the contribution of the work to the fields of visible-light photocatalytic activities were elaborated in detail. In our previous work, visible-light-responsive α/β-Bi_2O_3 nanowire catalysts were prepared via a facile in-situ hydrothermal process.[50] In order to improve the photocatalytic performance of α/β-Bi_2O_3 catalysts, the different plasmonic α/β-Bi_2O_3–Ag–AgCl photocatalysts have been successfully synthesized by anchoring Ag–AgCl nanocrystals on the surfaces of α/β-Bi_2O_3 nanowires via the deposition–precipitation method in assistance with the photo-reduction process. Especially, the significant improvement of the photocatalytic performance of α/β-Bi_2O_3 nanowires coupled with Ag-AgCl nanocrystals in the degradation of cationic rhodamine B (RhB) and acid orange 7 (AO7) under visible-light irradiation has been rarely reported. A plasmonic Z-scheme photocatalytic mechanism was proposed to explain the enhancement of the photocatalytic activity of the α/β-Bi_2O_3–Ag–AgCl composite photocatalyst on the basis of photocatalytic results. Hence, this work may be of interest to both materials scientists and those working in the area of catalyst design.

2. Experimental section

2.1 Synthesis of α/β-Bi_2O_3 nanowires

All chemicals were analytical grade and used without further purification. In a typical procedure, stochiometric amounts of $Bi(NO_3)_3 \cdot 5H_2O$ was dissolved in 15 mL of benzyl alcohol under vigorous stirring. Before being transferred to a Teflon-lined stainless autoclave (50 mL capacity). The

hydrothermal synthesis was conducted at 90~240 °C for 24 h in an electric oven. The system was then cooled to ambient temperature naturally. The as-prepared samples as precursors were collected and washed with distilled water and absolute alcohol several times, vacuum-dried, and then heated at 300 ^{o}C for 5 h to obtain α/β-Bi_2O_3 nanowires.

2.2 Synthesis of α/β-Bi_2O_3–Ag–AgCl composites

In a typical synthesis of α/β-Bi_2O_3–Ag–AgCl composites, 0.2 g of α/β-Bi_2O_3 nanowires and 0.3 g of CTAC were added to 100 mL of deionized water and the suspension was stirred for 60 min. Then 2.0 mL of 0.1 M $AgNO_3$ was quickly added to the above mixture. During this process, the excessive surfactant CTAC not only adsorbed onto the surface of α/β-Bi_2O_3, resulting in the homogenous disperse of AgCl nanocrystals due to the limitation of the number of nucleation sites for the growth of AgCl, but also induced Cl^- to precipitate Ag^+ in the suspension. The resulting suspension was stirred for 1.0 h and then placed under irradiation of 300 W Xe lamp for the indicated lengths of time. The suspension was filtered, washed with deionized water, and dried at 80 $^{\circ}$C for 12 h. Then the gray powder was calcined at 300 $^{\circ}$C for 3 h. Depending on the duration of irradiation, the as-prepared catalysts coupled with the 10wt% AgCl nanocrystals were denoted as α/β-Bi_2O_3–Ag–10wt%AgCl–m composites-m, where "m" represented 10, 30 and 50 min of photo-reduction time. Besides, the as-prepared catalysts under the photo-reduction process for 30 min were denoted as α/β-Bi_2O_3–Ag–nAgCl–30, where "n" represented 5, 10, 20, and 30wt% of the amount of AgCl nanocrystals in α/β-Bi_2O_3–Ag–AgCl composites.

2.3 Characterization

The obtained products were characterized by powder X-ray diffraction (XRD, MAC Science Co. Ltd Japan) using Cu Ka (λ = 0.1546 nm) and XRD patterns were obtained at 10^{o}~90^{o} by step scanning with a step size of 0.02^{o}. The morphology and size of the resultant products were observed

using a energy-dispersive spectra and transmission electron microscopy (TEM, JEM-2010). The optical properties of the samples were analyzed by UV-vis diffuse reflectance spectroscopy (UV-vis DRS) using a UV-vis spectrophotometer (UV-2550, Shimadzu) in the range 190–900 nm. The surface area of the samples were measured by TriStar 3000-BET/BJH Surface Area.

2.4 Photocatalytic test

Photocatalytic reactions were performed in an air-free, closed gas circulation system with a quartz reaction cell. Photocatalytic activity was evaluated by the degradation of rhodamine B (RhB) and acid orange 7 (AO7) in aqueous solution ($1*10^{-4}$ M, 100 mL) under visible-light irradiation using a 300 W Xe lamp with a cutoff filter ($\lambda > 420$ nm). A cylindrical Pyrex flask (200 mL) was placed in a sealed black box of which the top was open and the cutoff filter was set on the window face of the reaction vessel to ensure the desired irradiation condition. For the 0.1 g α/β-Bi_2O_3–Ag–AgCl composites as the catalysts were chosen for the evaluation of photocatalytic activity. Before illumination, the suspension between photocatalyst powders and rhodamine B (RhB) and acid orange 7 (AO7) at given time intervals (3 mL aliquots) were sampled and centrifuged to remove photocatalyst powders. The filtrates were analyzed by recording the variations of the absorption-band maximum (655 nm) in the UV-vis spectrum of RhB and AO7 dyes in aqueous solution using a UV-vis spectrophotometer (Shimadzu 2550, Japan).

3. Results and discussion

3.1 Characterization of α/β-Bi_2O_3–Ag–AgCl composites

Different plasmonic photocatalysts, have been attracted more attention due to its potential applications in the physical, chemical, biological, photoelectric, and catalytic fields. Fig. 1 shows the XRD patterns of the Ag/AgCl nanocrystals decorated the Bi_2O_3 catalysts. All the diffraction lines can be indexed as the α/β-Bi_2O_3 phase, cubic phase of AgCl and Ag, respectively. The major

phase can be indexed to the monoclinic α-Bi_2O_3 phase (PDF NO.4-294) while the little amount of second phase is recognized as the tetragonal β-Bi_2O_3 phase (PDF NO.18-244), demonstrating the formation of α-β phase heterojunction on Bi_2O_3, which is in agreement with the previous work.[50] Especially, after the photo-reduction of AgCl under UV-visible light for 10~30 min, three major diffraction peaks at 28.06°, 32.48° and 46.54° in the 2θ range of 10~80°, can be indexed to the (111), (200) and (220) reflections of a cubic silver chloride phase (space group: Fm3m [225]) according to the JCPDS card (No. 31-1238). Currently, as the irradiation time increased, the intensity of peaks of the AgCl phase decreased, indicating that parts of AgCl nanocrystals were photo-reduced, and the corresponding Ag nanoparticles were generated on the surface of α/β-Bi_2O_3–Ag–AgCl composites. However, there is no obvious reflections belonging to metal Ag species during this photo-reducing process for 10~20 min. Though the photoreduction for 30~50 min, the α/β-Bi_2O_3–Ag–AgCl composites shows a recognizable reflection at 2θ = 38.1° belonging to the metal Ag species in the XRD patterns. It is considered that the amount of the Ag species after the photo-induced process is too small to detect for the sample, which is in agreement with the previous reports.[40]

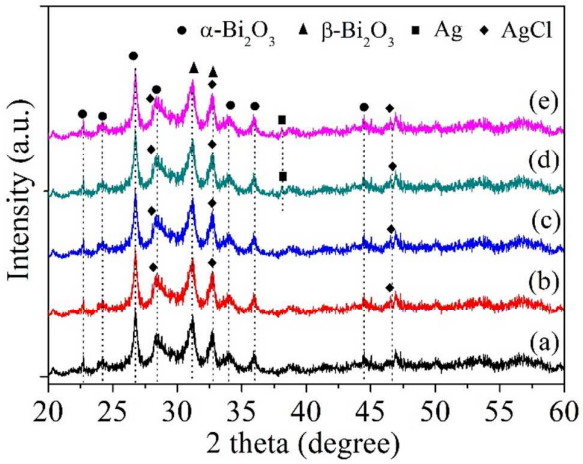

Fig. 1. XRD patterns of the α/β-Bi_2O_3–Ag–AgCl composites under the different photo-reduction times: (a) α/β-Bi_2O_3 nanowires; (b) α/β-Bi_2O_3–Ag–AgCl–10; (c) α/β-Bi_2O_3–Ag–AgCl–20; (d) α/β-Bi_2O_3–Ag–AgCl–30; and (e) α/β-Bi_2O_3–Ag–AgCl–50.

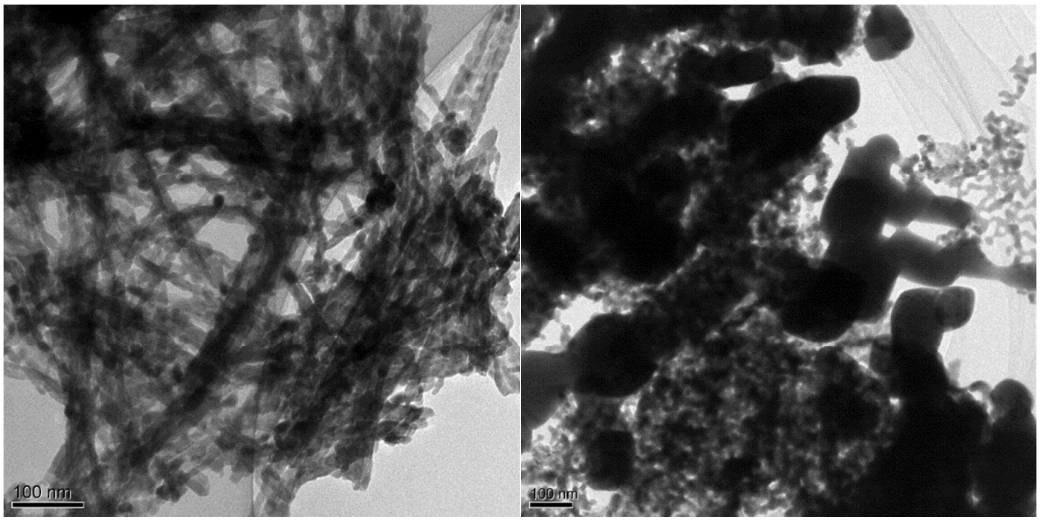

Fig. 2. TEM images of (a) α/β-Bi_2O_3 and (b) α/β-Bi_2O_3–Ag–10wt%AgCl–30 catalysts.

Typical TEM observations of the as-prepared hierarchical Ag–AgCl@α/β-Bi_2O_3 composites are shown in Fig. 2. As presented in Fig. 2a, the as-prepared sample consists of a large number of uniform α-Bi_2O_3 nanowires coupling with a little amount of β-Bi_2O_3 nanocrystals, which is in agreement with the previous work.[50] After the decoration, Fig. 2b indicates that the Ag/AgCl nanocrystals are uniformly and firmly anchored on the surfaces of the α/β-Bi_2O_3 nanowires. Besides, the corresponding Energy-dispersive X-ray spectra, the surface atomicratio of silver to chlorine was 1.4 times higher than the stoichio-metric ratio in AgCl (1: 1), indicating the existence of excessive Ag nanocrystals on the surface. As shown in Fig. 3A, it can be seen that the α/β-Bi_2O_3 samples are composed of Bi and O as the component elements and the Ag–AgCl nanocrystals consist of Ag, O, and Cl as the major elements. This hierarchical nanostructure is especially favorable for the enhancement of photocatalytic performance.

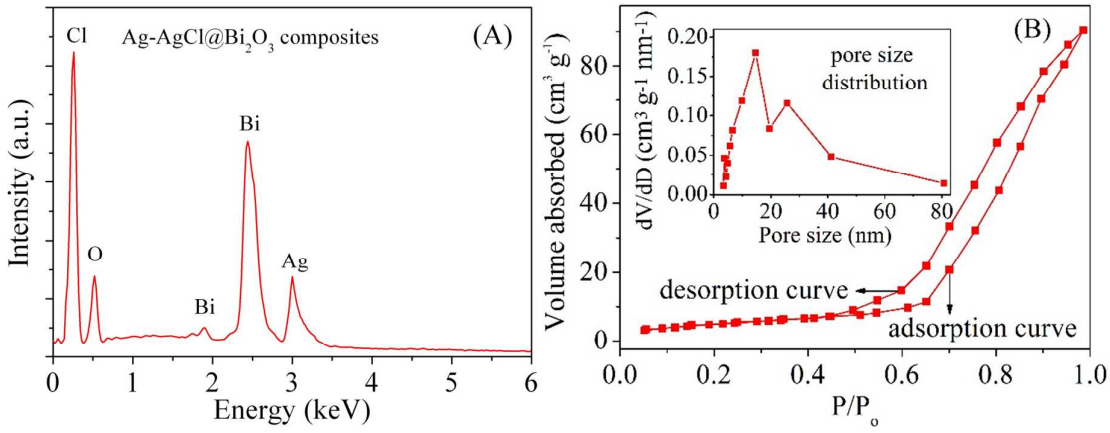

Fig. 3. (A) Energy-dispersive X-ray spectra, (B) Full nitrogen sorption isotherms and the inset is the corresponding pore-size distribution of the α/β-Bi_2O_3–Ag–%AgCl composites.

Full nitrogen sorption isotherms of the α/β-Bi_2O_3–Ag–AgCl composites were measured to gain the information about the specific surface area, as shown in Fig. 3B. The specific surface area was calculated to be 50 $m^2 g^{-1}$ by the BET equation. The corresponding Barrett Joyner Halenda (BJH) analysis (the inset in Fig. 3B) exhibit that most of the pores fall into the size range from 5 to 55 nm. These pores presumably arise from the spaces among the α/β-Bi_2O_3–Ag–AgCl composites. The high surface area and mesoporous structure of the α/β-Bi_2O_3–Ag–AgCl composites provide the possibility for the efficient diffusion and transportation of the degradable organic molecules and hydroxyl radicals in photochemical reaction, leading to the enhanced photocatalytic performance of the α/β-Bi_2O_3–Ag–AgCl composites.

3.2 Light absorption and photocatalytic activities of α/β-Bi_2O_3–Ag–AgCl composites

The optical absorption of the α/β-Bi_2O_3–Ag–AgCl composites was measured by UV-Vis diffuse reflection spectroscopy, as shown in Fig. 4. The α/β-Bi_2O_3–Ag–AgCl composites presented the wave length range up to 500 nm for the visible light absorption. For a crystalline semiconductor, the optical absorption near the band edge follows the equation.[51]

$$ahv = A\left(hv - E_g\right)^{n/2}$$

where a, n, E_g, and A are absorption coefficient, light frequency, band gap, and a constant, respectively. According to the equation above, the value of n for Bi_2O_3 is 1. The band gap energies of the α/β-Bi_2O_3 nanowires and α/β-Bi_2O_3–Ag–AgCl composites are determined from a plot of $(ahv)^2$ vs energy (hv) and are found to be about 2.4~2.8 eV, indicating that the mixed band gap energy of α-Bi_2O_3 (E_g = 2.71 eV) and β-Bi_2O_3 (E_g = 2.48 eV) heterojunction that have been confirmed in the previous work.[50] The series of α/β-Bi_2O_3–Ag–AgCl photocatalysts exhibited broad absorption in the region of visible light, which is attributed to the surface plasmon resonance effect of the Ag species formed in situ on the surfaces of the AgCl nanocrystals.[52] Thus, the hybridization of Ag–AgCl nanocrystals and the α/β-Bi_2O_3 nanowires is effective for the visible-light response of the composites, which is considered that the utilizing visible light for driving photocatalytic reactions is a key challenge and visible light absorption of a material is a prerequisite for visible light activity.

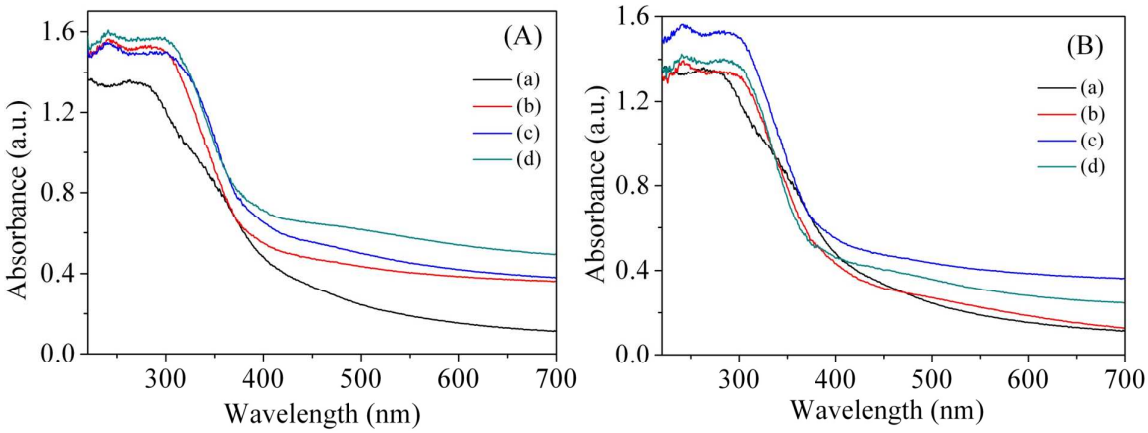

Fig. 4. The UV-Vis spectra of (A) α/β-Bi_2O_3–Ag–nAgCl–30 using with different amount of Ag–AgCl: (a) 0, (b) 10wt%, (c) 20wt%, (d) 30wt%; (B) α/β-Bi_2O_3–Ag–10wt%AgCl–m under various photo-reduction time: (a) 0, (b) 10 min, (c) 30 min and (d) 50 min.

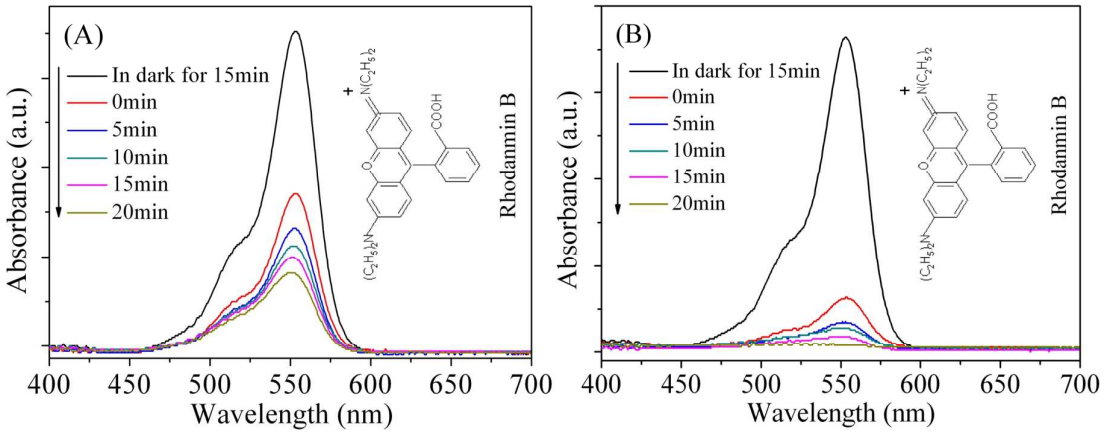

Fig. 5. UV-visible spectra changes in the RhB degradation using different samples. (A) as-prepared α/β-Bi_2O_3 nanowires and (B) the α/β-Bi_2O_3–Ag–10wt%AgCl–30 photocatalysts under visible-ligh irradiation.

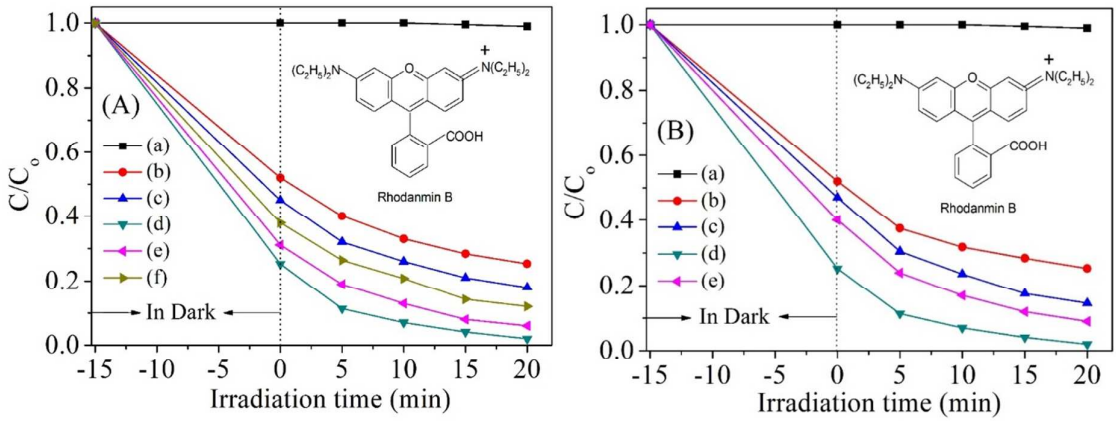

Fig. 6. Visible-light photocatalytic degradation of RhB solution for (A) α/β-Bi_2O_3–Ag–nAgCl–30 using with different amount of Ag–AgCl: (a) RhB solution without catalyst, (b) 0wt%, (c) 5wt%, (d) 10wt%, (e) 20wt%, (f) 30wt%; (B) α/β-Bi_2O_3–Ag–10wt%AgCl–m under various photo-reduction time: (a) RhB solution without catalyst, (b) 0 min, (c) 10 min, (d) 30 min and (e) 50 min.

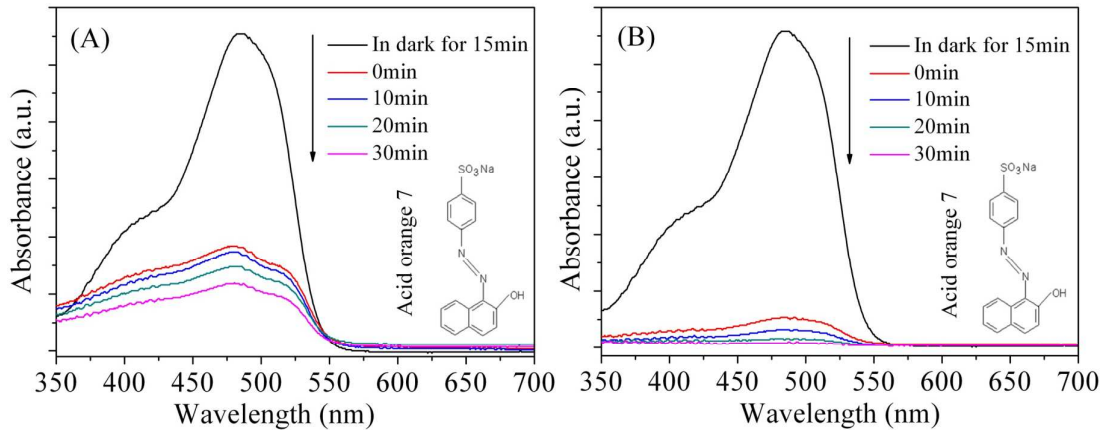

Fig. 7. UV-visible spectra changes in the OA7 degradation with (A) the α/β-Bi_2O_3 and (B) the α/β-Bi_2O_3–Ag–10wt%AgCl–30 photocatalysts under visible-light irradiation.

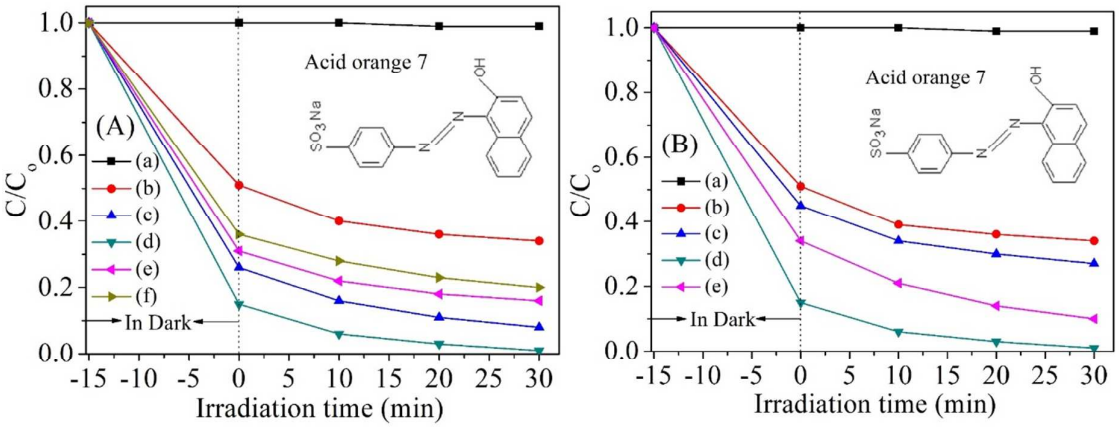

Fig. 8. Photocatalytic degradation of OA7 solution for (A) α/β-Bi_2O_3–Ag–nAgCl–30 using with different amount of Ag–AgCl: (a) OA7 solution without catalyst, (b) 0wt%, (c) 5wt%, (d) 10wt%, (e) 20wt%, (f) 30wt%; (B) α/β-Bi_2O_3–Ag–10wt%AgCl–m under various photo-reduction time: (a) OA7 solution without catalyst, (b) 0 min, (c) 10 min, (d) 30 min and (e) 50 min.

The photocatalytic performance of the α/β-Bi_2O_3 and α/β-Bi_2O_3–Ag–AgCl composites samples were evaluated by monitoring the decomposition of rhodamine B (RhB) and acid orange 7 (AO7) in an aqueous solution under visible light irradiation, respectively. The time-dependent UV–vis absorption spectra of RhB and AO7 dyes during the visible-light irradiation are displayed in Fig. 5

and Fig. 7. Fig. 6 and Fig. 8 show the different photodegradation efficiencies of RhB and AO7 solutions as a function of irradiation time for the various α/β-Bi_2O_3–Ag–AgCl samples. Firstly, the results for RhB degradation show that after visible-light irradiation, the photocatalytic activities for the α/β-Bi_2O_3–Ag–nAgCl–30 samples after the photo-reduction time for 30 min, increased with the increasing amount of Ag–AgCl nanocrystals up to 10wt%. However, the photocatalytic performance for RhB degradation decreased with the increasing amount of Ag–AgCl nanocrystals from 10wt% to 30wt%. Secondly, the results for RhB degradation present that the photocatalytic performance for the α/β-Bi_2O_3–Ag–10wt%AgCl–m samples coupled with a certain amount of Ag–AgCl nanocrystals (10wt%) under the different photo-reduction time, increased with the increasing photo-reduction time from 10 to 30 min after visible-light irradiation. In addition, the photocatalytic activity for RhB degradation decreased with the increase of photo-reduction time up to 50 min. Furthermore, the photocatalytic performance of the α/β-Bi_2O_3–Ag–nAgCl–m samples for the AO7 degradation present the same tendency, as shown in Fig. 7 and Fig. 8. Among these samples, theα/β-Bi_2O_3–Ag–10wt%AgCl–30 photocatalysts exhibited the most pronounced photocatalytic activity with the highest RhB and AO7 degradation efficiencies of about 98% (irradiation for 25 min) and 99% (irradiation for 30 min), respectively. As the duration of photo-reduction and the amount of Ag–AgCl nanocrystals increased, the Ag nanoparticles content increased correspondingly, changing of the ratios of Ag^0/Ag^+, which has an intimate relationship with the photocatalytic performance. In addition, the various α/β-Bi_2O_3–Ag–20wt%AgCl–30, α/β-Bi_2O_3–Ag–30wt%AgCl–30 and α/β-Bi_2O_3–Ag–10wt%AgCl–50 samples show the relative lower efficiencies in photocatalytic activities for the degradation of RhB and AO7 dyes solution. More details about photocatalytic efficiencies of α/β-Bi_2O_3–Ag–AgCl composites have been shown in Table 1. In addition, the blank experiments were also carried out in the presence of irradiation

without α/β-Bi_2O_3–Ag–AgCl samples, indicating that there is no apparent change for the degradation of RhB and AO7 dyes under visible light irradiation in the absence of photocatalysts. Besides, the adsorption capacities of RhB molecules on α/β-Bi_2O_3–Ag–AgCl nanostructures coupled with different amount of Ag–AgCl nanocrystals for 0, 5, 10, 20 and 30wt% are approaching 48%, 55%, 75%, 69% and 62%, respectively. And the adsorption capacities of AO7 molecules on α/β-Bi_2O_3–Ag–AgCl nanostructures under the various photo-reduction time for 0, 10, 30 and 50 min are reaching 49%, 55%, 85%, and 66%, respectively, which is ascribed to the high surface area of the α/β-Bi_2O_3–Ag–AgCl nanostructures. Compared to the previous reports,[20-40] the as-prepared α/β-Bi_2O_3–Ag–AgCl nanostructures exhibit the superior photocatalytic degradation performance of RhB and AO7 molecules. In order to examine the elemental composition, chemical status, and the content of elements of the α/β-Bi_2O_3–Ag–10wt%AgCl–30 composite after photocatalytic reduction were examined by X-ray photoelectron spectroscopy. In the XPS spectra in Fig. 9 of the Ag 3d regions of the α/β-Bi_2O_3–Ag–10wt%AgCl–30 sample, two peaks are observed at approximately 367.4 and 373.6 eV in each spectrum, which are ascribed to the Ag $3d_{5/2}$ and Ag $3d_{3/2}$ binding energies, respectively. These two peaks could be further deconvoluted into two peaks, at about 367.3/368.4 eV, and 373.6/374.6 eV, respectively. The peaks at 367.3 and 373.6 eV are attributed to Ag^+ of AgCl, and those at 368.4 and 374.6 eV are ascribed to the metal Ag^0. According to the results of the curve-fitting of Ag3d XPS spectrum, the atom ratio of metallic Ag to Ag^+ in the α/β-Bi_2O_3–Ag–AgCl composite is calculated to be 1:1.4. However, the ratio of Ag^0/Ag^+ increased as the duration of photo-reduction increased from 10 to 50 min, indicating that the excessive amount of silver might have been produced from the photo-reduction of AgCl on the surface. That is why the α/β-Bi_2O_3–Ag–10wt%AgCl–50 sample with the more content of the Ag^0 on the surface of the sample, shows lower efficiency in photocatalytic activity. Thus, the enhancement of

photocatalytic performance of the α/β-Bi_2O_3–Ag–10wt%AgCl–30 composite is ascribed to the roles of Ag–AgCl nanocrystals.

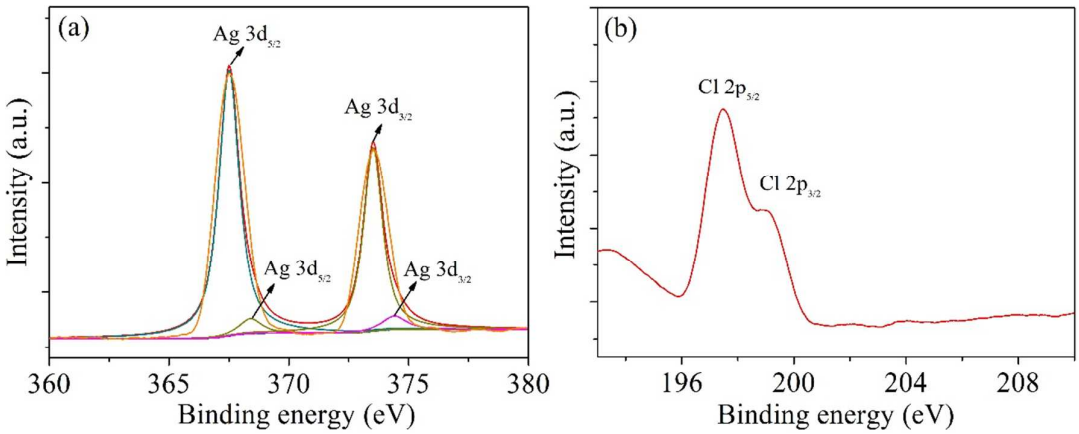

Fig. 9. XPS spectra of (a) Ag 3d and (b) Cl 2p for the α/β-Bi_2O_3–Ag–AgCl composites.

Table 1. Photocatalytic performance of as-prepared α/β–Bi_2O_3–Ag–AgCl composites with the different amount of Ag–AgCl nanocrystals and the various photo-reduction time for the degradation of RhB (irradiation for 20 min) and AO7 (irradiation for 30 min) dyes.

Samples	Ag–AgCl amount	Photo-reduction time	Degradation efficiency (RhB dye)	Kinetic rate (RhB dye)	Degradation efficiency (AO7 dye)	Kinetic rate (AO7 dye)
S1	0wt%	30min	75%	0.03567	66%	0.01296
S2	5wt%	30min	82%	0.04508	92%	0.03911
S3	10wt%	30min	98%	0.12196	99%	0.08817
S4	20wt%	30min	94%	0.08312	84%	0.02185
S5	30wt%	30min	88%	0.05793	80%	0.01960
S6	10wt%	10min	85%	0.05776	73%	0.01658
S7	10wt%	50min	91%	0.07353	90%	0.04077

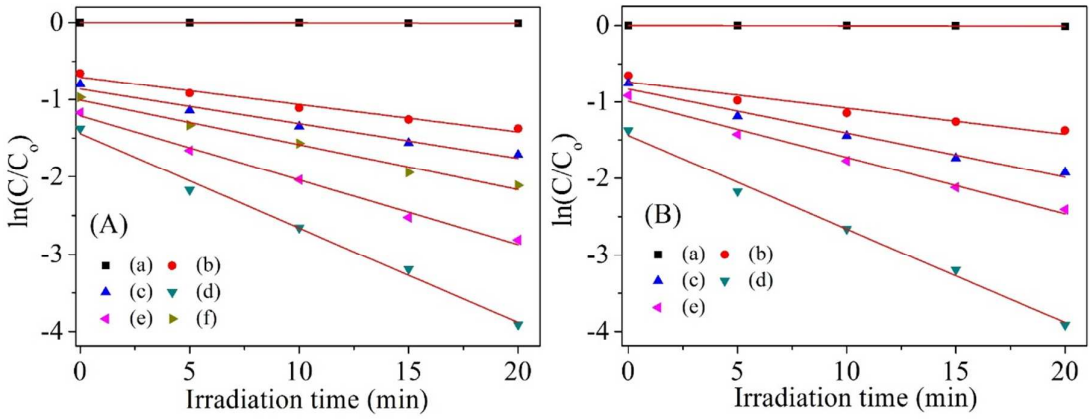

Fig. 10. Photocatalytic degradation kinetic rates of RhB solution for (A) α/β-Bi_2O_3–Ag–nAgCl–30 using with different amount of Ag–AgCl: (a) RhB solution without catalyst, (b) 0wt%, (c) 5wt%, (d) 10wt%, (e) 20wt%, (f) 30wt%; (B) α/β-Bi_2O_3–Ag–10wt%AgCl–m under various photo-reduction time: (a) RhB solution without catalyst, (b) 0 min, (c) 10 min, (d) 30 min and (e) 50 min.

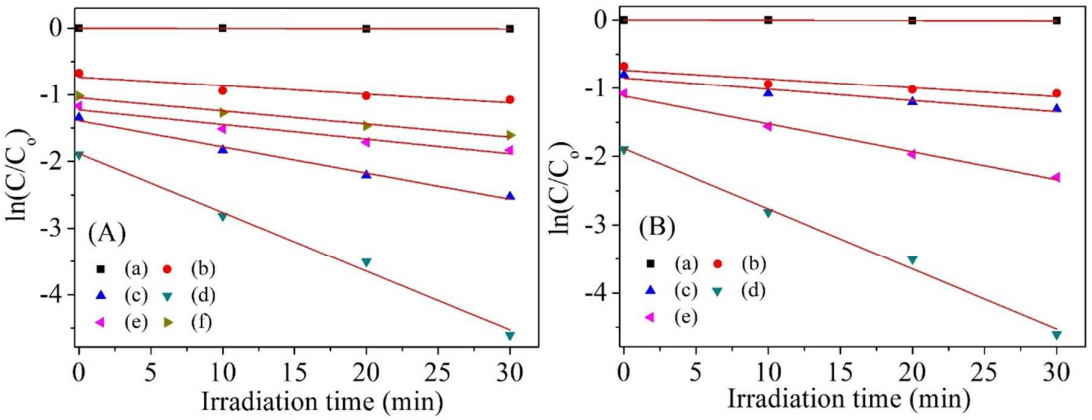

Fig. 11. Photocatalytic degradation kinetic rates of OA7 solution for (A) α/β-Bi_2O_3–Ag–nAgCl–30 using with different amount of Ag–AgCl: (a) OA7 solution without catalyst, (b) 0wt%, (c) 5wt%, (d) 10wt%, (e) 20wt%, (f) 30wt%; (B) α/β-Bi_2O_3–Ag–10wt%AgCl–m under various photo-reduction time: (a) OA7 solution without catalyst, (b) 0 min, (c) 10 min, (d) 30 min and (e) 50 min.

Generally, the decomposition of the dye could be assigned to a pseudo–first–order kinetics reaction with a simplified Langmuir–Hinshelwood model when C_o is very small.

$$\ln(C_o/C) = kt$$

where k is the apparent first–order kinetics rate constant, and was determined from a linear fit to the data as shown in Fig. 10 and Fig. 11. Clearly, the degradating kinetics rate of RhB molecules on α/β-Bi_2O_3–Ag–10wt%AgCl–30 nanostructures coupled with different amount of Ag–AgCl nanocrystals for 0, 5, 10, 20 and 30wt% are approaching 0.03567, 0.04508, 0.12196, 0.08312 and 0.05793, respectively. Besides, it is obvious that the kinetics rate of the degradation of AO7 molecules on α/β-Bi_2O_3–Ag–10wt%AgCl–30 nanostructures under the various photo-reduction time for 0, 10, 30 and 50 min are approaching 0.01296, 0.01658, 0.08817, and 0.04077, respectively.

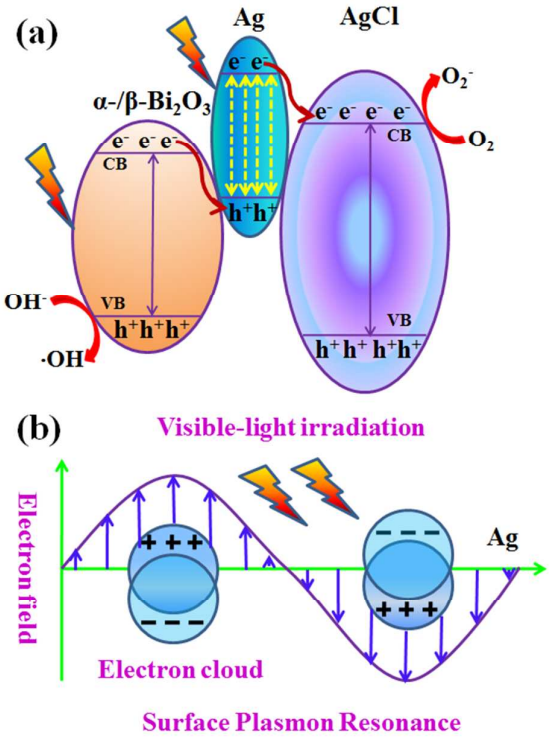

Fig. 12. (a) Schematic illustration of the charge separation and transfer in the plasmonic Z-scheme α/β-Bi_2O_3–Ag–AgCl composites; (b) schematic for the surface plasmon resonance effect of Ag nanocrystals in the α/β-Bi_2O_3–Ag–AgCl composites.

The recycling properties of the α/β-Bi_2O_3–Ag–10wt%AgCl–30 photocatalysts for RhB and AO7 solutions under visible-light irradiation (λ > 420 nm), as shown in Fig. 1S (Supporting Information), demonstrating a fairly stable photocatalytic performance for RhB and AO7 photodegradation. After a recycling application of three times, there is almost no obvious change for the photocatalytic activity of the α/β-Bi_2O_3–Ag–AgCl photocatalyst. The XRD pattern of the α/β-Bi_2O_3–Ag–AgCl sample after the recycling use indicates that the Ag content slightly increases but the major phases are still the AgCl and α/β-Bi_2O_3 phases, as shown in Fig. 2S (Supporting Information).

To further understand the mechanism for the remarkably enhanced photocatalytic performance of the α/β-Bi_2O_3–Ag–AgCl photocatalysts from the following aspects. Firstly, the existence of Ag/AgCl nanocrystals on the surfaces of the α/β-Bi_2O_3 nanowires forms the uniquely hierarchical nanostructure, which provides a large number of interfaces between the Ag/AgCl and α/β-Bi_2O_3 species. The profuse interfaces are accessible to the outer environment, and provide numerous active sites for the photodegradation of dye molecules. Based on above-mentioned results, the adsorption and photosensitization contributed much in the decolorization of the organic dyes. Secondly, the metal Ag clusters formed in situ on the semiconductors AgCl and the α/β-Bi_2O_3 nanocrystals remarkably enhance the absorption in the visible light region due to the surface plasmonic resonance effect, as shown in Fig. 12, which photogenerates transient holes that can oxidize the dye molecules.[52] Last but not least, the positively synergistic effects of the coupling of Ag/AgCl and the α/β-Bi_2O_3 nanowires improve the effective separation of the photo-generated electron–hole pairs, and the possible transfer routes of the photo-generated electrons and holes are also introduced to explain the enhanced photocatalytic activity using the conduction band minimum (CBM) and valence band maximum (VBM) potentials of Ag/AgCl and α/β-Bi_2O_3. Due to the surface plasmonic resonance effect and dipolar character of metallic Ag, metallic Ag can absorb visible light, and the

absorbed photon would be efficiently separated to the photo-generated electrons and holes.[53-59] Under visible-light irradiation, both Ag nanocrystals and α/β-Bi_2O_3 can absorb visible-light photons to produce photogenerated electrons and holes. The plasmon-induced electrons of Ag nanocrystals are injected into the CB of AgCl to reduce oxygen, while the holes remain on the Ag nanocrystals. As for α/β-Bi_2O_3, the photogenerated electrons transfer to the Ag nanocrystals to recombine with the plasmon-induced holes produced by plasmonic absorption of Ag nanocrystals, while the VB holes remain on α/β-Bi_2O_3 to oxidize organic substances. Therefore, the reduction active site is on the CB of AgCl while the oxidation active site is on the VB of α/β-Bi_2O_3 for the α/β-Bi_2O_3–Ag–AgCl composite.

4. Conclusion

The plasmonic Z-scheme α/β-Bi_2O_3–Ag–AgCl photocatalysts have been successfully synthesized by anchoring Ag–AgCl nanocrystals on the surfaces of α/β-Bi_2O_3 nanowires via the deposition–precipitation method and photo-reduction process. The amount and the photo-reduction time of Ag–AgCl nanocrystals for the α/β-Bi_2O_3–Ag–AgCl composites have appreciable effects on their photocatalytic performance. The 10wt% Ag–AgCl nanocrystals with the photo-reduction time for 30 min, displayed the highest photocatalytic activity over the degradation of rhodamine B and acid orange 7 dyes. The enhanced photocatalytic performance is attributed to (i) the hierarchical structures with high opening surface areas and profuse interfacial active sites, (ii) the enhanced absorption of visible light due to the surface plasmonic resonance effect of Ag clusters, and (iii) the positively synergistic effects of the AgCl and α/β-Bi_2O_3 in effective separation of photo-generated electrons and holes for the plasmonic Z-scheme α/β-Bi_2O_3–Ag–AgCl composites. This work opens

a cost-effective and facile way to achieve highly efficient photocatalysts with promising applications in environmental purification and energy conversion.

Acknowledgements

This work was supported by National Science Foundation of China (No. 51102015) and Beijing High School Youth Talent Plan (YETP0351).

References

1. X. Chen, S. Mao, Chem. Rev., 2007, 107, 2891–2959.
2. J. G. Hou, R. Cao, Z. Wang, S. Q. Jiao, H. M. Zhu, J. Hazard. Mater., 2012, 217-218, 177–186.
3. R. Kozhummal, Y. Yang, F. Güder, A. Hartel, X. Lu, U. M. Küçükbayrak, A. Mateo-Alonso, M. Elwenspoek, M. Zacharias, ACS Nano, 2012, 6, 7133–7141.
4. J. G. Hou, Z. Wang, S. Q. Jiao, H. M. Zhu, CrystEngComm, 2012, 14, 5923–5928.
5. A. Kudo, Y. Miseki, Chem. Soc. Rev., 2009, 38, 253–278.
6. K. Maeda, K. Teramura, D. Lu, T. Takata, N. Saito, Y. Inoue, K. Domen, Nature, 2006, 440, 295–295.
7. Z. G. Yi, J. H. Ye, N. Kikugawa, T. Kako, S. X. Ouyang, H. Stuart-Williams, H. Yang, J. Y. Cao, W. J. Luo, Z. S. Li, Y. Liu, R. L. Withers, Nat. Mater., 2010, 9, 559–564.
8. J. G. Hou, R. Cao, Z. Wang, S. Q. Jiao, H. M. Zhu, Dalton T., 2011, 40, 4038–4041.
9. X. C. Wang, K. Maeda, A. Thomas, K. Takanabe, G. Xin, J. M. Carlsson, K. Domen, M. Antonietti, Nat. Mater., 2009, 8, 76–82.
10. J. G. Hou, Z. Wang, W. B. Kan, S. Q. Jiao, H. M. Zhu, R. V. Kumar, J. Mater. Chem., 2012, 22, 7291–7299.

11. G. Liu, H. G. Yang, X. W. Wang, L. N. Cheng, J. Pan, G. Q. Lu, H. M. Cheng, J. Am. Chem. Soc., 2009, 131, 12868–12869.

12. Q. J. Xiang, J. G. Yu, W. G. Wang, M. Jaroniec, Chem. Commun., 2011, 47, 6906–6908.

13. G. Liu, C.H. Sun, S. C. Smith, L. Z. Wang, G. Q. Lu, H. M. Cheng, J. Colloid Interface Sci., 2010, 349, 477–483.

14. J. G. Yu, G. P. Dai, Q. J. Xiang, M. Jaroniec, J. Mater. Chem., 2011, 2, 1049–1057.

15. J. W. Tang, Z. G Zou, J. H. Ye, Angew. Chem. Int. Edit., 2004, 43, 4463–4466.

16. W. J. Luo, Z. S. Yang, Z. S Li, J. Y. Zhang, J. G. Liu, Z. Y. Zhao, Z. Q. Wang, S. C. Yan, T. Yu, Z. G. Zou, Energ. Environ. Sci., 2011, 4, 4046–4051.

17. L. Zhou, W. Z. Wang, S. W. Liu, J. Mol. Catal. A Chem., 2006, 252, 120–124.

18. G. K. Zhang, J. L. Yang, S. M. Zhang, Q. Xiong, B. B. Huang, J. T. Wang, W. Q. Gong, J. Hazard. Mater., 2009, 172, 986–992.

19. X. Q. Zhu, J.L. Zhang, F. Chen, Appl. Catal. B, 2011, 102, 316–322.

20. J. G. Hou, Y.F. Qu, D. Krsmanovic, C. Ducati, D. Eder, R. V. Kumar, J. Mater. Chem., 2010, 20, 2418–2423.

21. J. G. Hou, R. Cao, S. Q. Jiao, H. M. Zhu, R.V. Kumar, Appl. Catal. B, 2011, 104, 399–406.

22. J. G. Hou, R. Cao, Z. Wang, S. Q. Jiao, H. M. Zhu, J. Mater. Chem., 2011, 11, 7296–7301.

23. J. G. Hou, Y. F. Qu, D. Krsmanovic, C. Ducati, D. Eder, R. V. Kumar, Chem. Commun., 2009, 26, 3937–3939.

24. L. S. Zhang, W. Z. Wang, Z. L. Zhou, Small, 2007, 3, 1618–1625.

25. L. S. Zhang, W. Z. Wang, J. Yang, Z. G. Chen, W. Q. Zhang, L. Zhou, S. W. Liu, Appl. Catal. A, 2006, 308, 105–110.

26. M. Drache, P. Roussel, J. P. Wignacourt, Chem. Rev., 2007, 107, 80–96.

27. H. F. Cheng, B. B. Huang, J. B. Lu, Z. Y. Wang, B. Xu, X. Y. Qin, X. Y. Zhang, Y. Dai, Phys. Chem. Chem. Phys., 2010, 12, 15468–15475.

28. J. C. Yu, A. W. Xu, L. Z. Zhang, R. Q. Song, L. Wu, J. Phys. Chem. B, 2004, 108, 64–70.

29. H. Abdul, M. Tiziano, G. Valentina. J. Am. Chem. Soc., 2008,130, 9658–9659.

30. J. In, I. Yoon, K. Seo, J. Park, J. Choo, Y. Lee, B. Kim, Chem. Eur. J., 2011, 17, 1304–1309.

31. Y. F. Qiu, M. L. Yang, H. B. Fan, Y. Z. Zuo, Y. Y. Shao, Y. J. Xu, X. X. Yang, S. H. Yang, CrystEngComm, 2011, 13, 1843–1850.

32. Y. F. Qiu, D. F. Liu, J. H. Yang, S. H. Yang, Adv. Mater., 2006, 18, 2604–2608.

33. L. Zhou, W. Z. Wang, H.L. Xu, S. M. Sun, M. Shang, Chem. Eur. J., 2009, 18, 1776–1782.

34. M. Muruganandham, R. Amutha, G. J. Lee, S. H. Hsieh, J. J. Wu, M. Sillanpää, J. Phys. Chem. C, 2012, 116, 12906–12915.

35. K. Brezesinski, R. Ostermann, P. Hartmann, J. Perlich, T. Brezesinski, Chem. Mater., 2010, 22, 3079–3085.

36. Q. Q. Huang, S. N. Zhang, C. X. Cai, B. Zhou, Mater. Lett., 2011, 65, 988–990.

37. J. G. Hou, Z. Wang, S. Q. Jiao, H. M. Zhu, J. Hazard. Mater., 2011, 192, 1772–1779.

38. D. Tsukamoto, Y. Shiraishi, Y. Sugano, S. Ichikawa, S. Tanaka, T. Hirai, J. Am. Chem. Soc., 2012, 134, 6309–6315.

39. W. A. Murray W.L. Barnes, Adv. Mater., 2007, 19, 3771–3782.

40. L. Q. Ye, J. Y. Liu, C. Q. Gong, L. H. Tian, T. Y. Peng, L. Zan, ACS Catal., 2012, 2, 1677–1683.

41. J. F. Guo, B. Ma, A. Yin, K. Fan, W. L. Dai, J. Hazard. Mater., 2012, 211–212, 77–82.

42. D. L. Chen, T. Li, Q. Q. Chen, J. B. Gao, B. B. Fan, J. Li, X. J. Li, R. Zhang, J. Sun, L. Gao, Nanoscale, 2012, 4, 5431–5439.

43. G. Tian, Y. Chen, H. L. Bao, X. Meng, K. Pan, W. Zhou, C. Tian, J. Q. Wang, H.G. Fu, J. Mater.

Chem., 2012, 22, 2081–2088.

45. Y. G. Xu, H. Xu, H. M. Li, J. X. Xia, C. T. Liu, L. Liu, J. Alloys Compd., 2011, 509, 3286–3292.

46. H. G. Yua, R. Liu, X. F. Wang, P. Wang, J. G. Yu, Appl. Catal. B, 2012, 111–112, 326–333.

47. W. Xiong, Q. Zhao, X. Li, D. Zhang, Catal. Commun., 2011, 16, 229–233.

48. J. G. Hou, C. Yang, Z. Wang, Q. H. Ji, Y. Li, S. Q. Jiao, H. M. Zhu, Appl. Catal. B, 2013, 142–143, 579-589.

49. Y. P. Bi, S.X. Ouyang, J. Y. Cao, J. H. Ye, Phys. Chem. Chem. Phys., 2011, 13, 10071–10075.

50. J. G. Hou, C. Yang, Z. Wang, W. L. Zhou, S. Q. Jiao, H. M. Zhu, Appl. Catal. B, 2013, 142-143, 504-511.

51. M. A. Butler, J. Appl. Phys., 1977, 48, 1914–1920.

52. J. Lan, X. Zhou, G. Liu, J. Yu, J. Zhang, L. Zhi, G. Nie, Nanoscale, 2011, 3, 5161–5167.

53. R. Liu, P. Wang, X. F. Wang, H. G. Yu, J. G. Yu, J. Phys. Chem. C, 2012, 116, 17721–17728.

54. S. Linic, P. Christopher, D. B. Ingram, Nat. Mater., 2011, 10, 911–921.

55. J. G. Hou, C. Yang, Z. Wang, S. Q. Jiao, H. M. Zhu. Appl. Catal. B, 2013, 129, 333–341.

56. P. Zhou, J. G. Yu, M. Jaroniec, Adv. Mater. 2014, DOI: 10.1002/adma.201400288.

57 J. G. Yu, S. H. Wang, J. X. Low and W. Xiao, Phys. Chem. Chem. Phys., 2013, 15, 16883–16890.

58 L. Yang, H. Zhou, T. Fan and D. Zhang, Phys. Chem. Chem. Phys., 2014, 16, 6810–6826.

59 Y. Yang, W. Guo, Y. Guo, Y. Zhao, X. Yuan, Y. Guo, J. Hazard. Mater. 2014, 271, 150–159.

Graphical Abstract

The plasmonic Z-scheme α/β-Bi_2O_3–Ag–AgCl photocatalysts were successfully synthesized and their photocatalytic performance for the degradation of rhodamine B and acid orange 7 dyes were systematically investigated.